

Iron Alloy Fischer-Tropsch Catalysts

I. Oxidation-Reduction Studies of the Fe-Ni System

E. E. UNMUTH,¹ L. H. SCHWARTZ,² AND J. B. BUTT³

Ipatieff Laboratory, Northwestern University, Evanston, Illinois 60201

Received February 19, 1979; revised July 24, 1979

The oxidation and reduction behavior of a series of Fe/SiO₂, Ni/SiO₂, and 4Fe:Ni/SiO₂ catalysts, each with total metals loading of 5 wt%, has been investigated. Characterization methods employed were Mössbauer effect spectroscopy, X-ray diffraction, and temperature-programmed reduction. Reduction of the nickel (H₂, 425°C, 12 hr) proceeds directly to the metal and is essentially quantitative, while reduction of α -Fe₂O₃ under the same conditions proceeds via the intermediate Fe₃O₄ and yields about 70% metallic iron. Reduction of 4Fe:Ni results in a biphasic mixture of BCC and FCC alloys, with a nickel FCC phase of ca. 37.5 atom% Ni, which is approximately the bulk equilibrium value. Finally, there are some changes in particle size and granularity upon oxidation and reduction in all cases. Details of these alterations are discussed.

INTRODUCTION

In a recent study (1) we reported some data concerning the oxidation-reduction behavior of an Fe/SiO₂ catalyst as characterized by Mössbauer spectroscopy and X-ray diffraction. This catalyst was also observed to carburize under synthesis reaction conditions (1 atm, 3:1-H₂:CO, 250°C), a result which has also recently been reported by Delgass and Raupp (2) for Fe/SiO₂. The formation of carbides is important in determining the activity and selectivity of iron-based synthesis catalysts, and this in turn is affected by the method of preparation and pretreatment employed. Thus, it is appropriate to investigate the oxidation-reduction behavior of these materials as well. We report here a study for the iron-nickel system with three catalysts, Fe/SiO₂, 4Fe:Ni/SiO₂, and Ni/SiO₂, all with a total metals loading of approximately 5 wt%. Characterization methods employed were Mössbauer spectroscopy (MES), X-ray diffraction (XRD), and tem-

perature-programmed reduction (TPR). Subsequent papers will present details of the reaction of these three catalysts at 1 atm, 3:1-H₂:CO, 255°C and the implications of these results in understanding Fischer-Tropsch synthesis.

EXPERIMENTAL SECTION

Catalysts. The samples were prepared by impregnation of 80-100 mesh Davison 62 silica gel to incipient wetness with the appropriate aqueous solution of the nitrate salt. Simultaneous impregnation was used in preparation of the bimetallic. After drying at 125°C overnight the samples were calcined in air at 200°C for 2 hr and then at 450°C for 4 hr. Details of the procedure have been described previously (1); in Table 1 are listed the catalysts so prepared.

Mössbauer spectra. Spectra were obtained with a constant acceleration spectrometer using a ⁵⁷Co source electroplated on a 12- μ m rhodium foil. Oxidation and reduction studies were carried out *in situ* in a controlled atmosphere cell described in detail by Unmuth (3).

X-ray diffraction. All measurements were made on a Phillips diffractometer equipped with a diffracted beam graphite monochro-

¹ Present address: Amoco Oil Company, Naperville, Ill. 60540.

² Department of Materials Science and Engineering.

³ Department of Chemical Engineering.

TABLE I
Catalysts Prepared

Designation	Loading (wt%) ^a	Particle diameter (nm) ^b
Fe/SiO ₂	4.94	13.3 ± 0.5
4Fe : Ni/SiO ₂	3.41(Fe); 0.83(Ni)	12.8 ± 0.5(BCC); 8.9 ± 0.5(FCC)
Ni/SiO ₂	4.58	16.9 ± 1

^a Based on reduced metal.

^b Via X-ray line broadening after reduction in H₂, 425°C, 24 hr.

meter using CuK_α radiation. Particle sizes were estimated using the Scherrer formula (4) and assuming that particle size and instrumental broadening are Gaussian.

Temperature-programmed reactor. Oxidation-reduction cycles were followed gravimetrically with a Cahn RG electrobalance contained in a Pyrex chamber with sample and counterbalance hang-down tubes connected via ground glass joints. A Lindberg Model 54241-S tube furnace was fitted around the sample tube and a Theal Model TP-2000 temperature programmed used for control. Thermal lags at the sample were such that linearity of the temperature program was significantly affected, so a chromel-alumel thermocouple was located within 1 cm of the sample for temperature measurement. The precision of the balance is better than 1 in 10⁶ with a maximum sensitivity of 0.1 μg. Typical sample sizes were approximately 100 mg, allowing a maximum precision of 0.1 μg (3). Weight-time and time derivative of weight were measured; precision in these values is estimated to be within 0.4 μg/min. A schematic diagram of the entire apparatus is given in Fig. 1.

Oxidation-reduction sequences. A standard sequence of oxidation and reduction was used for the samples studied by MES and XRD. After calcination to form the initial oxide and spectral characterization,⁴

the samples were reduced in H₂ at 425°C for either 12 or 24 hr, and the measurements were again made. The reduced samples were then subjected to reoxidation in air at 200°C for 2 hr, spectra were recorded, then further oxidized at 425°C for an additional 2 hr, spectra recorded, and finally, the reoxidized sample which had initially been reduced 425°C, 24 hr was again reduced in H₂, 425°C, 12 hr, and the spectra recorded. Similar results were obtained for 12- and 24-hr reductions; 24-hr data are presented here unless stated otherwise.

In the TPR experiments, the initial oxide catalyst was dried under vacuum at 450°C, 0.5 hr, cooled to room temperature, purged with helium, and hydrogen flow was initiated. After displacement of helium, the temperature program was started and weight loss, rate of weight loss, and temperature were recorded. Programming rates ranging from about 5 to 25°C/min were employed for each sample, allowing evaluation of activation energies from peak position (5); maximum temperatures were from 500 to 600°C. In some experiments the starting material was not the initial oxide but a 425°C, 24-hr reduced sample reoxidized in the 200, 425°C sequence described above. Also, some TPR experiments were terminated after appearance of a peak and the sample was characterized by MES or XRD.

⁴ Mössbauer samples were reduced *in situ*, while X-ray samples were reduced external to the diffractometer and then transferred. We have shown previously (1) that Fe/SiO₂ is not bulk reoxidized on exposure to air for short times at room temperature.

RESULTS-GENERAL

The results described in this section deal first with the MES and XRD studies and second with the TPR experiments.

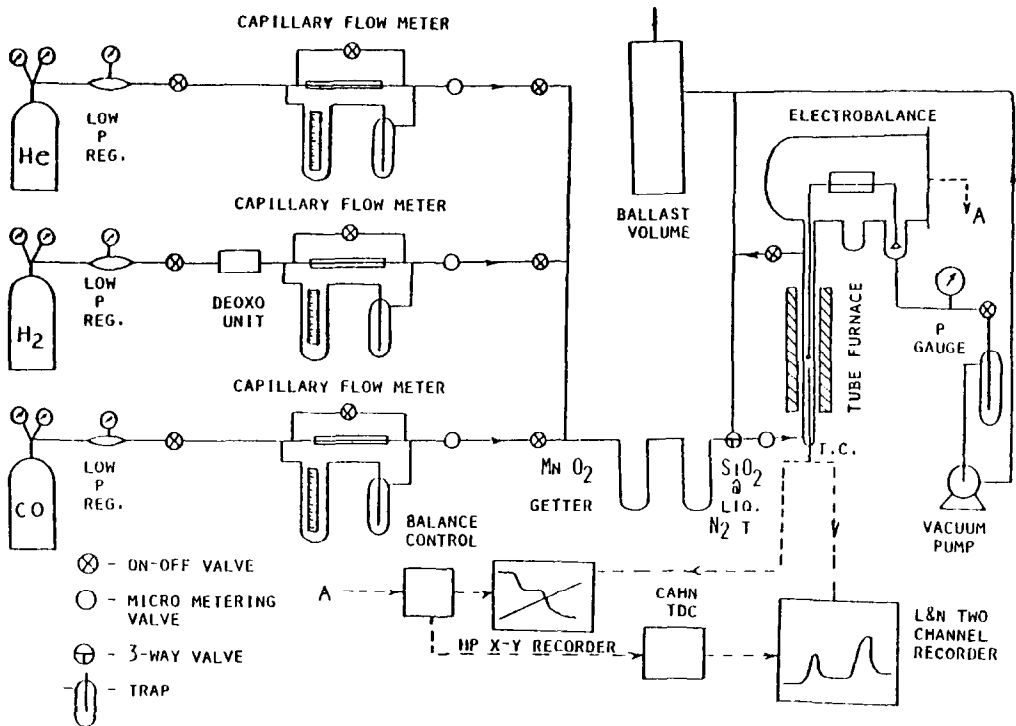


FIG. 1. Schematic of temperature-programmed apparatus.

Oxidation-Reduction, Mössbauer, and X-Ray Results

Fe/SiO₂. Basic MES data on oxidation-reduction of the 4.84% Fe/SiO₂ have been discussed previously by Amelse *et al.* (1). In summary, the initial oxide after calcination is α -Fe₂O₃ characterized by a magnetically split six line pattern superimposed over a broad non-Lorentzian central peak of unclear origin. XRD confirms that the initial oxide is α -Fe₂O₃ by comparison with JCPDS data (6). The experimental hyperfine field of 503 ± 1 kOe is smaller than the 517 kOe normally quoted (7); however apparent hyperfine field is a function of particle size for small particles of α -Fe₂O₃. The measured field corresponds to a particle size of 18.0 nm (8, 9); this is in excellent agreement with X-ray results which give 17.8 ± 0.5 nm from the average of the first three low-angle reflections.

After either 12- or 24-hr reduction, 425°C, MES (Fig. 2) indicates the presence

of α -Fe as well as small amounts of an unidentified paramagnetic species. There is evidence from the TPR experiments to be discussed that this is in part attributable to superparamagnetic Fe₃O₄ resulting from partial reduction of small particles of Fe₂O₃. The extent of reduction was calculated from the areas of the magnetically

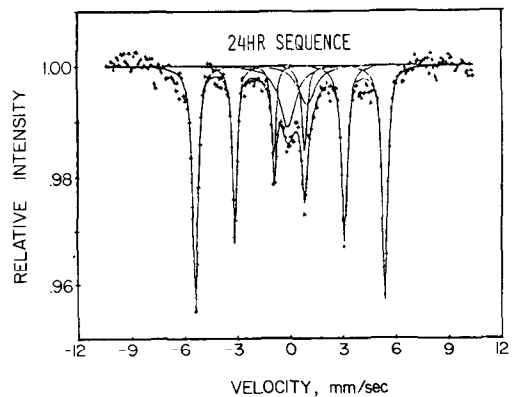


FIG. 2. Mössbauer spectrum of 24 hr, 425°C reduced Fe/SiO₂.

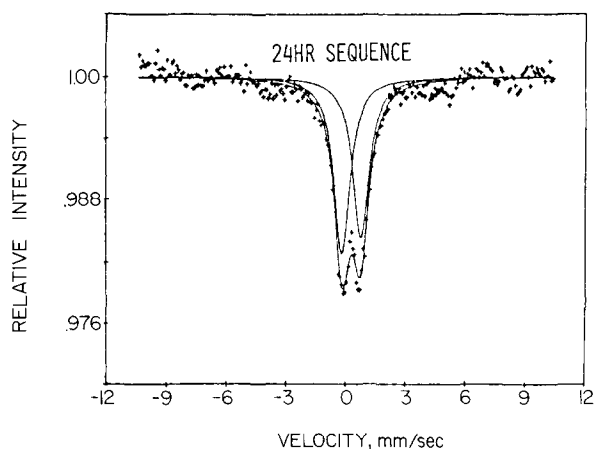


FIG. 3. Mössbauer spectrum of 2 hr, 200°C reoxidized Fe/SiO₂.

split and the quadrupole split oxide patterns using 0.7 (10) for the ratio of recoil free fractions of Fe₃O₄/Fe. Calculated reductions for 12- and 24-hr treatments were 67 and 69%, respectively, with average particle sizes also essentially the same, 12.9 ± 0.5 nm (12 hr) and 13.3 ± 0.5 nm (24 hr). These results agree qualitatively with the observation of Hobson and Gager (11) that superparamagnetic α-Fe₂O₃/SiO₂ cannot be reduced to the metallic state. Similar observations have been made by Delgass and Raupp (2). Our previous interpretation of the spectra of reduced Fe/SiO₂ was based on the assumption of unreduced superparamagnetic Fe₂O₃, and the computed extents of reduction somewhat higher (1). At the moment the identity of the oxide phase in the reduced catalysts remains unresolved and is being investigated.

Upon air reoxidation at 200°C, 2 hr, a primarily superparamagnetic oxide is formed, illustrated in Fig. 3. Using the correlation between quadrupole splitting and particle size of Kündig *et al.* (8) for α-Fe₂O₃, we determine an average particle size of less than 5 nm. The XRD pattern and MES isomer shifts confirm that the reoxidized phase consists of small particles of α-Fe₂O₃, 2.9 ± 1 nm, for both reduction sequences. Further oxidation at 425°C, 2 hr, decreased the superparamagnetic portion of the Mössbauer spectra, indicating

some growth in the oxide particle size. X-ray results are in agreement, with average particle sizes of about 4.1 ± 1 nm for both samples. The quadrupole splitting for the reoxidized samples was considerably larger than for the initial α-Fe₂O₃. Particle sizes obtained via MES agreed with those obtained from XRD within a factor of two for all treatments; however, the XRD results are believed to be more reliable.

4Fe : Ni/SiO₂. The iron-nickel catalyst, 3.41% Fe and 0.83% Ni, is 18.72 atom% Ni. The MES for the initial oxide catalyst is given in Fig. 4, and comparison between the hyperfine parameters of the initial Fe/SiO₂ and 4Fe : Ni/SiO₂ oxides reveals that the iron environments of the two are similar. Differences are more apparent in comparison of half line widths of the peaks in which significant broadening of the iron-nickel MES peaks suggest that at least some iron atoms have nickel nearest neighbors mixed in the α-Fe₂O₃ phase. The XRD pattern indicates the presence of both an α-Fe₂O₃ rhombohedral phase and a NiO cubic phase. Estimation of relative composition from the ratio of the integrated intensities of the reflections for the two phases (3) indicated the cubic phase to be less than 4 vol% of the oxide. Hence, most of the Ni is in the rhombohedral phase. This material is designated α-Fe_{2-ξ}Ni_ξO₃, where ξ can be as high as 0.37 for this formulation.

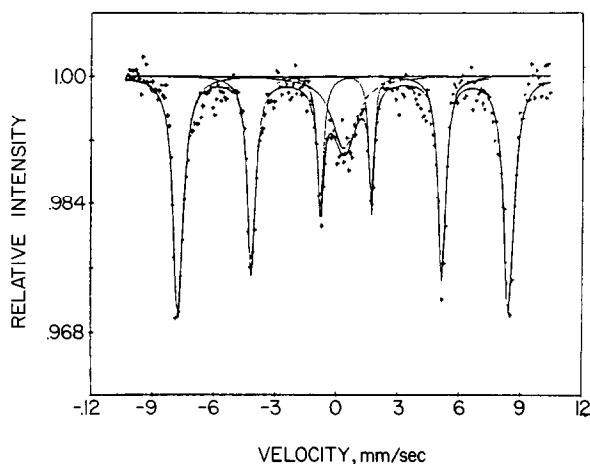


FIG. 4. Mössbauer spectrum of initial oxide, 4Fe:Ni/SiO₂.

A bulk metallic alloy of the composition of this Fe-Ni catalyst, prepared at 425°C and cooled to room temperature, should contain two phases: an FCC alloy at ~38% Ni and a BCC alloy at ~6% Ni (12). The Mössbauer spectrum of H₂, 425°C, 24 hr, 4Fe:Ni/SiO₂ shown in Fig. 5 reflects the formation of two phases on reduction; this was verified by XRD where the measured d-spacings indicated the presence of both FCC and BCC alloys. The nickel content of the supported BCC phase was estimated from the hyperfine field, H, of the spectrum of the reduced catalyst, using the data on Vincze *et al.* (13) on the effect of Ni con-

centration on H in the BCC alloy. The measured H = 340 ± 1 kOe corresponds to 14 ± 4 atom% Ni. The nickel content of the FCC phase was estimated from the measured lattice parameter, a₀, and data on lattice parameters vs composition given by Pearson (14). For H₂, 425°C, 12 hr, a₀ = 0.3593 ± 0.0002 corresponds to 44.5 ± 5 atom% Ni, while for H₂, 425°C, 24 hr, a₀ = 0.3596 ± 0.0002 corresponds to 37.5 ± 5 atom% Ni. Relative amounts of the two phases were determined from the integrated intensities of the XRD peaks and converted to volume fraction using tabulated lattice parameters. For the 12-hr re-

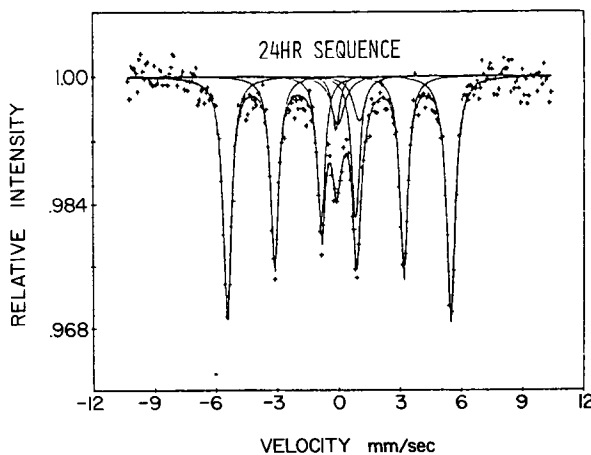


FIG. 5. Mössbauer spectrum of 24 hr, 425°C reduced 4Fe:Ni/SiO₂.

duction 17.0 ± 5 atom% of the metal is in the FCC phase while for the 24-hr reduction 24.3 ± 1.5 atom% is FCC.

An attempt was also made to determine the relative phase distribution from Mössbauer data, assuming that the magnetically split spectrum corresponds to the BCC phase and the single central peak to the FCC phase (15). This estimate turned out to be significantly different from the XRD value (more BCC, less FCC). This is probably because MES distinguishes between magnetic and nonmagnetic iron, rather than BCC and FCC. Johnson *et al.* (16) have shown that the hyperfine fields for FCC iron-nickel alloys fall rapidly to zero for Ni concentrations below about 40 atom%. The presence of a small amount of paramagnetic metal can then be understood as a consequence of composition variation within the FCC phase; however, no quantitative estimate of this variation is possible.

The oxide content of the reduced samples can be determined from relative Mössbauer areas, assuming the ratio of recoil-free fractions of the metal to the oxide phases is as for α -Fe/Fe₂O₄. The consistency of compositions and phase distributions can be checked via material balance as shown in Table 2. The closure of the balance is quite good, especially since both MES and XRD data are employed in the analysis. Initially it was assumed that all the nickel was reduced and only iron remained in the oxide phase; however, it is unlikely that nickel is completely removed because of the low diffusivity of nickel in the oxide matrix (3). Hence, if the mismatch in the nickel balance is attributed to unreduced nickel the composition of the oxide phase, taken to be a mixed magnetite Fe_{3- ψ} Ni _{ψ} O₄, can be determined; these values of ψ are also reported in Table 2.

The value of 37.5% Ni in the FCC phase for H₂, 425°C, 24 hr, is very close to the equilibrium value of 38% for the bulk alloy (12) and provides some evidence that the two phases are in intimate contact. The possible morphology of the individual

TABLE 2
Material Balance for Reduced 4Fe: Ni/SiO₂

Property	H ₂ , 425°C, 12 hr	H ₂ , 425°C, 24 hr
atom% Ni in FCC	44.5	37.5
atom% Ni in BCC	14.0	14.0
atom% metal reduced	84.10	88.75
atom% metal phase, FCC	17.0	24.3
atom% BCC alloy ^a	69.44	72.57
atom% FCC alloy ^a	14.24	23.23
atom% unreduced metal ^a	16.32	12.63
Percentage error, Fe balance ^a	0.0	1.4
Percentage error, Ni balance ^a	-16.4	-6.6
Percentage magneti- cally split spectrum	77.73	82.85
Percentage unsplit spectrum	5.95	7.94
ψ in Fe _{3-ψ} Ni _{ψ} O ₄ ^b	0.41	0.30

^a Calculated from the material balance.

^b Calculated from the mismatch in the material balance.

phases has been discussed in detail by Unmuth (3). While the evidence suggests that both phases are present in all particles, no information from either MES or XRD indicates whether surface segregation occurs. Four samples of H₂, 425°C, 24 hr catalyst examined via Auger spectroscopy (Physical Electronics, SAM 590A) gave an average iron surface concentration of 82.5% (17), within experimental error of the overall Fe composition of 81.3%.

Reoxidation at 200°C, 2 hr, and 425°C, 2 hr, results in the formation of superparamagnetic particles as evidenced by MES showing predominantly a quadrupole split doublet (similar to Fig. 3). As for Fe/SiO₂, this is the result of a decrease in particle size; XRD results are given in Table 3. The ratio of initial to final particle volumes yields a measure of the grains per particle formed in the reoxidation (Table 3). The MES parameters for both reoxidized Fe/SiO₂ and 4Fe: Ni/SiO₂ were similar, indicating similarity in the reoxidized

TABLE 3
Reoxidation Results: 4Fe : Ni/SiO₂

Treatment	Phase	Average particle diameter (nm)		
		Initial	Final	Grains/ particle
(1) H ₂ , 425°C, 12 hr	α -Fe _{2-ϵ} Ni _{ϵ} O ₃	13.9 \pm .5	5.8 \pm 1	14
O ₂ , 425°C, 2 hr	NiO	6.2 \pm 1	6.2 \pm 1	1
(2) H ₂ , 425°C, 24 hr	α -Fe _{2-ϵ} Ni _{ϵ} O ₃	13.9 \pm .5	5.5 \pm 1	16
O ₂ , 425°C, 2 hr	NiO	6.2 \pm 1	4.7 \pm 1	2

states. However, the diffraction patterns for the two reoxidized catalysts indicate an increase in NiO with respect to the initial oxide; for 4Fe:Ni/SiO₂ this change is about a factor of two.

Ni/SiO₂. Nickel oxide is much easier to reduce than iron oxide; given sufficient reduction time one would expect nickel metal since the ratio of the equilibrium constants is approximately 700 to 400°C (18). However, difficulties can be encountered in reduction if silicates are formed during calcination in preparation.

Comparison of the XRD patterns with tabulated JCPDS d-spacings indicates that the initial oxide phase is NiO; there is no evidence of the formation of nickel silicate, but a small amount could be obscured by peak broadening. In contrast to the iron and iron-nickel samples, the NiO particles were not spherical and, at 17.2 nm, were somewhat larger than the average pore diameter of the support, 14 nm (19). Treatment in H₂, 12 or 24 hr, 425°C gave complete reductions (particle sizes 15.1 and 16.9 nm, respectively); the somewhat larger particle size for the 24-hr reduction suggests the presence of sintering. Upon reoxidation, the average particle sizes were reduced by a factor of almost 2, but again showed no evidence of nickel silicate formation.

Secondary Reduction

Each of the samples was subjected to a second reduction following initial reduction

of the original oxide and subsequent oxidation. These results are informative as to the processes of granule formation and dispersion.

Fe/SiO₂. The particle size of the original α -Fe₂O₃/SiO₂ was 17.9 nm and the average of the 12- and 24-hr reduced sample 13.1 nm, a reduction in size of about 27%. That computed from bulk density change for α -Fe₂O₃ to α -Fe is 22%, thus the oxide particles appear to reduce directly to metal with little sintering. Oxidation of the 12-hr reduced Fe/SiO₂ in two stages first reduces particle size from 13.1 to 2.9 nm (O₂, 200°C, 2 hr) and then increases particles size to 4.2 nm (O₂, 425°C, 2 hr). Rereduction of this 4.2-nm oxide particle resulted in α -Fe/SiO₂ with a particle size of 14.5 nm, comparable to that produced via reduction of the initial oxide. This cycle of particle sizes implies that the reoxidized materials consist of large particles of agglomerated crystallites produced from a single large reduced metal particle. The amount of iron is constant since there is no transport between particles, hence the granularity (number of grains per initial oxide particle) can be estimated by dividing the initial crystallite volume by the reoxidized crystal volume. This is given in Table 4, and a schematic of the oxidation-reduction cycle for Fe/SiO₂ is shown in Fig. 6. Increased granularity upon oxidation is very well known for bulk metal oxidation (20). Oxidation of a transition metal normally occurs through nucleation and growth of the oxide phase at the

TABLE 4
Variations in Granularity; α -Fe₂O₃/SiO₂

	Initial oxide	O ₂ , 200°C, 2 hr	O ₂ , 425°C, 2 hr
12-hr reduction	1	235	77
24-hr reduction	1	235	90

surface of the metal, each nucleation site resulting in a separate oxide grain. High temperature treatment leads to grain growth, as shown by the differences between 200 and 425°C oxidation here. It is significant that rereduction of the calcined oxide produces approximately the same metallic crystallite as that from reduction of the initial oxide and no sintering or dispersion is observed.

4Fe : Ni/SiO₂. The H₂, 425°C, 24 hr sample was rereduced at 425°C, 12 hr, after the standard oxidation sequence. Generally the same pattern of behavior was found as for Fe/SiO₂; results of the Mössbauer and X-ray analysis are presented in Table 5. As with Fe/SiO₂, the rereduced particle size is slightly larger than the reduced initial oxide, so it again seems that the apparent change in the particle size upon reoxidation is due to an increase in granularity and not redispersion (see Table 3). The FCC content of the rereduced metal phase is approximately 17%, in good agreement with that found for H₂, 425°C, 12 hr of the initial oxide. A summary of the oxidation-reduction history of *4Fe : Ni/SiO₂* is given in Fig. 7.

Ni/SiO₂. The reoxidized catalyst was re-

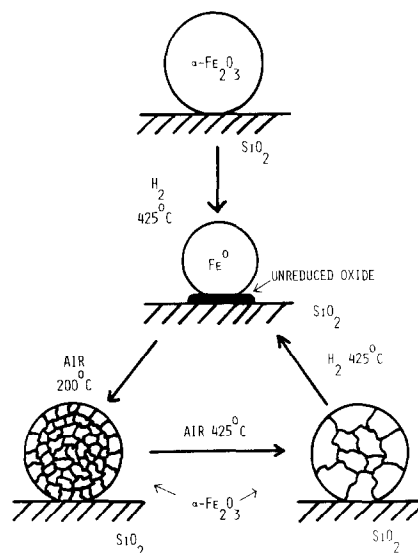


FIG. 6. Oxidation-reduction history of Fe/SiO₂.

reduced, H₂, 425°C, 12 hr which yielded a particle diameter of 13.5 ± 1 nm, about 20% smaller than that obtained on reduction of the original oxide. This is most likely the result of some redispersion of the initially reduced metal when it is reoxidized; hence reoxidation of the supported nickel is characterized by some redispersion rather than an increase in particle granularity. The evidence for redispersion is also supported by the nonspherical shape of the particles for this catalyst, both oxidized and reduced. Since reduction occurs via the same mechanism of cationic diffusion as oxidation, it might be expected that the morphology of the metal catalyst would mimic in some way that of its oxide precursor. Evidence for this is provided in Table 6. The

TABLE 5
Rereduction of *4Fe : Ni/SiO₂*

Phase	Particle diameter (nm) H ₂ , 425°C, 24 (initial)	H ₂ , 425°C, 12 (reduction)	Rereduced phase composition %Ni
BCC	12.8 ± 0.5	14.2 ± 0.5	14
FCC	8.9 ± 1	10.1 ± 1	37
Atom% reduced	88	85	

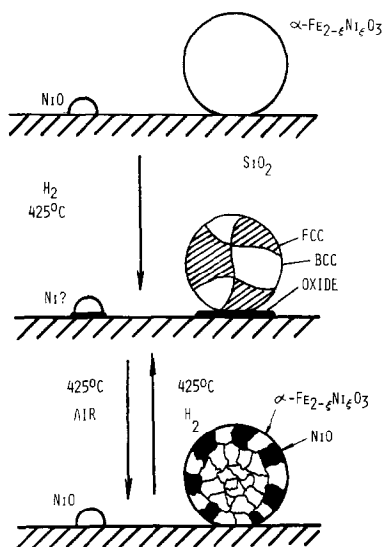


FIG. 7. Oxidation-reduction history of 4Fe: Ni/SiO₂.

(220) size is smaller than the (111) size for both initial oxide and reduced metal and, except for the initial oxide, the (111) size is greater than the (200) size by a relatively constant factor. Upon reduction sintering produces some redistribution of the metal and increased wetting of the support. Thus the reoxidized particle shape is similar to reduced metal, but redispersion occurring during reoxidation causes a more complete spreading of the oxide over the support. The reduction of this oxide then results in a more highly dispersed metal than that found upon reduction of the initial oxide. A schematic for the oxidation-reduction cycle for Ni/SiO₂ is given in Fig. 8.

TABLE 6

Particles Sizes for Ni/SiO₂ (nm)

Sample	Reflection		
	(111)	(200)	(220)
(1) Initial oxide	16.4 ± 0.5	17.9 ± 0.5	14.0 ± 0.5
(2) H ₂ , 425°C, 12 hr	16.3 ± 0.5	14.0 ± 0.5	14.9 ± 0.5
(3) H ₂ , 425°C, 24 hr	18.2 ± 0.5	16.2 ± 0.5	16.3 ± 0.5
(4) H ₂ , 425°C, 24 hr O ₂ , 425°C, 2 hr	9.6 ± 1	7.9 ± 1	—
(5) H ₂ , 425°C, 24 hr O ₂ , 425°C, 2 hr H ₂ , 425°C, 12 hr	14.9 ± 0.5	12.0 ± 0.5	—

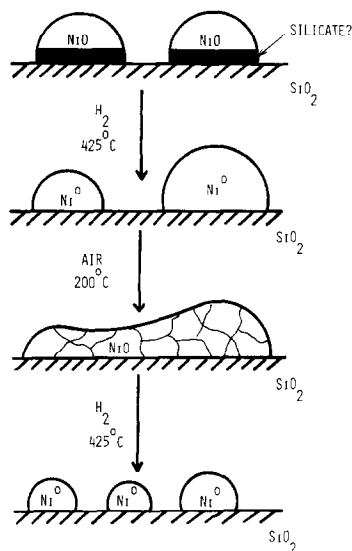


FIG. 8. Oxidation-reduction history of Ni/SiO₂.

Temperature-Programmed Reduction

Oxidation-reduction studies provide information concerning the state of reduction and morphology at specific points in the cycle, but little data on the mechanism of reduction during the process. Thermogravimetric analysis has been commonly employed for investigation of the reduction of transition metal oxides, although the temperature-programmed technique has not been used much for catalytic studies. The method turns out to be very useful in providing information on the number of reduction paths and their activation energies, the extent of reduction, and the number of oxide phases.

Fe/SiO₂ The relative TPR profiles for Fe/SiO₂ at three different programming rates are shown in Fig. 9 and the positions and magnitudes of the maxima in rate in Table 7. The phase diagram for Fe-O (21) suggests that reduction of α-Fe₂O₃ near equilibrium conditions should be quantitative to Fe₃O₄ before final reduction to metallic Fe. FeO is not encountered in our experiments since the temperature never exceeded 570°C. To identify the reactions corresponding to the α and β peaks, MES was recorded for TPR samples removed

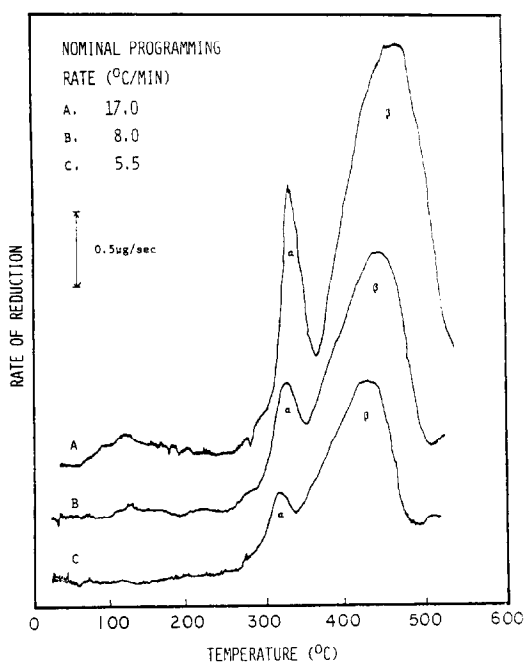
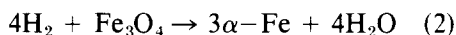
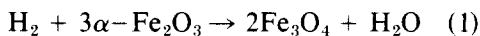


FIG. 9. Temperature-programmed reduction of Fe/SiO₂.

after each peak. The spectrum of the α peak sample was well characterized by parameters for Fe₃O₄; the absence of any detectable α -Fe₂O₃ spectrum indicated complete conversion to Fe₃O₄. The spectrum of the β peak sample was that of α -Fe metal. Hence for this two-stage reduction:



A comparison between measured weight changes and those computed from the stoichiometry of Eq. (1) for the α peak is given in Table 7. Reasonable agreement is obtained, assuming the α peak to be symmetric.

The stoichiometry was also determined at an arbitrarily selected temperature of 485°C for each of the programming rates to determine the extent of reduction (defined as the atomic percent of cations reduced to metal). This is essentially a linear function of programming rate, ranging from 46.5% for 17°C/min to 76.7% for 5.5°C/min, assuming that the remaining oxide is Fe₃O₄. The results of subsequent isothermal studies have not exceeded 80% reduction (22). Evidence for the Fe₃O₄ intermediate in reduction of bulk α -Fe₂O₃ has been given by Gazzarini and Lanzavecchia (23) and Colombo *et al.* (24) for low temperature (200–300°C) reduction. Differences in detailed kinetic behavior of the reductions were functions of grain area, lattice defects, and particle size, but it appears that the presence of the support here does not alter the general sequence of reduction deduced from bulk oxide studies.

Ni/SiO₂. TPR profiles for Ni/SiO₂ are shown in Fig. 10 and the pertinent experimental parameters given in Table 8. The three peaks are a surprise since one would expect direct reduction to metal. Examination of a sample removed at the minimum,

TABLE 7

TPR Data for Fe/SiO₂

Profile	Peak	T (°C)	(-r) × 10 ² O ² /sec-nm	α Peak, (mole O ²⁻ /mole Fe) ^a
A (17.0°C/min)	α	354.3 ± 0.5	14.5 ± 0.5 ^b	1.35 ± 0.05
	β	493.3 ± 0.5	21.1 ± 0.5	
B (8.0°C/min)	α	343.2 ± 0.5	5.5 ± 0.5	1.37 ± 0.05
	β	471.5 ± 0.5	14.7 ± 0.5	
C (5.5°C/min)	α	332.9 ± 0.5	3.4 ± 0.5	1.38 ± 0.05
	β	450.3 ± 0.5	11.1 ± 0.5	

^a This ratio for Fe₂O₃ is 1.33.

^b Rates are based on surface area of initial oxide catalyst calculated from X-ray diffraction particle size assuming spherical particle shapes.

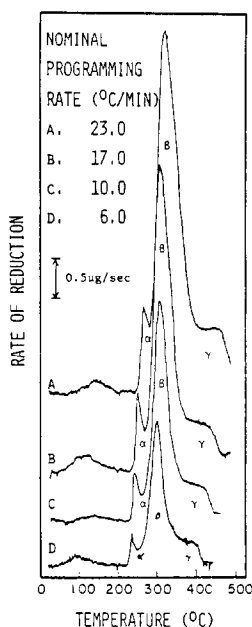
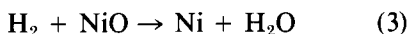


FIG. 10. Temperature-programmed reduction of Ni/SiO₂.

α , revealed that the initial grey NiO had turned a sea-green color, which reverted to grey as the sample cooled. XRD indicated the presence only of Ni and NiO. Both Keely and Maynor (25) and Szekely *et al.* (26) indicate a crystallographic phase transition in the region of 250°C, reported previously as transformation of a rhombohedral NiO structure to a cubic NaCl structure above 200°C (14). The temperature corresponding to α decreased with programming rate and the value of $262 \pm 1^\circ\text{C}$ for the lowest rate is in good agreement with the value of 257°C reported by Szekeley *et al.* Thus the first peak is the result of an endothermic phase transition occurring simultaneously with reduction of the NiO.

The β peak was verified by XRD to be Ni metal, so the reduction reaction is directly:



The shoulder on β is thought to be due to very small particles of oxide or, possibly, silicate, involving strong support interactions. About 25 atom% of the nickel is affected as estimated by material balance

from the TPR profiles. It is not possible to distinguish between oxide or silicate here, owing to the broad XRD peaks. The extent of reduction at 485°C is reported in Table 8; whatever is the nature of the interaction with silica it is not strong enough to prevent complete reduction under these conditions.

A reoxidized Ni/SiO₂ catalyst was compared in TPR with the original oxide, shown in Fig. 11. The major feature is the nearly complete disappearance of the α and γ peaks of the initial oxide. Absence of α , coupled with the fact that the reoxidized catalyst was a light green-gray color, suggests that the cubic phase is stabilized at room temperature by the reoxidation procedure, although phase identification via XRD was inconclusive due to the similarities in the broadened rhombohedral and cubic patterns. Disappearance of γ implies that support interactions were much weaker on the reoxidized catalyst. Since this catalyst is more dispersed than the initial oxide, it can be argued that support interaction leading to γ is via silicate. In the initial reduction all of the nickel including the silicate is eventually reduced. Evidently the reoxidation conditions used here are not severe enough for the silicate to reform. Finally, the absolute value of the maximum rate at β for the reoxidized sample was

TABLE 8

TPR Data, for Ni/SiO₂

Profile	Peak	T (°C)	$(-r) \times 10^2$ O ²⁻ /sec-nm ^{2a}	Percentage reduction at 485°C
A (23°C/min)	α	289 ± 1		101.9 ± 2
	β	334 ± 0.5	56.8 ± 5	
	γ	460 ± 10		
B (17°C/min)	α	277 ± 1		101.8 ± 2
	β	322 ± 0.5	49.1 ± 5	
	γ	415 ± 10		
C (10°C/min)	α	271 ± 1		99.5 ± 2
	β	319 ± 0.5	35.2 ± 4	
	γ	403 ± 10		
D (6°C/min)	α	262 ± 1		90.2 ± 2
	β	310 ± 0.5	24.3 ± 2	
	γ	390 ± 10		

^a Rates based on surface area of initial oxide catalyst.

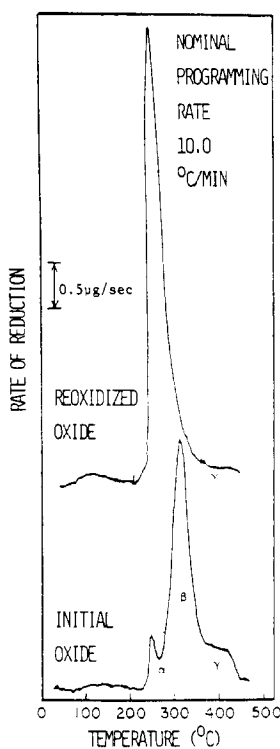


FIG. 11. Temperature-programmed reduction of 2 hr, 200°C reoxidized Ni/SiO₂.

almost twice that of the initial oxide. This is almost certainly the result of the combination of increased dispersion and the increased amount of easily reduced oxide in the reoxidized catalyst.

4Fe:Ni/SiO₂. The TPR profiles for 4Fe:Ni/SiO₂ are shown in Fig. 12a with corresponding parameters in Table 9. A high temperature peak β , with a low-temperature shoulder, α , is observed for all programming rates. A comparison among the profiles for all three materials is given in Fig. 12b at 12°C/min. The profile for 4Fe:Ni/SiO₂ is suggestive of the reduction of a single oxide phase, and the reduction appears similar to Fe/SiO₂ with the β peak shifted to a slightly lower temperature.

Mössbauer spectra were recorded for samples reduced just past both the α and β peaks for 4Fe:Ni/SiO₂, and these were compared with those of the initial oxide and the α transition of Fe/SiO₂ (α peak) and

reduced Fe/SiO₂ (β peak). Comparison of the α peak sample revealed quantitative conversion of the initial α -Fe_{2- ξ} Ni _{ξ} O₃ to an inverse spinel phase with Fe³⁺ in octahedral and tetrahedral sites and Fe²⁺ only in octahedral sites. The fraction of octahedral iron in the 4Fe:Ni/SiO₂ was smaller than that for the Fe/SiO₂ so nickel occupies predominantly octahedral sites in the spinel. This has been reported in other studies of the Fe-Ni system (27). The spectrum of the β peak sample was that of reduced metal.

Reducibility data are also reported in Table 9 and indicate nearly full reduction to the metal phase for the lowest program rates. Reduction of the 4Fe:Ni/SiO₂ was always greater than that of Fe/SiO₂ at equivalent programming rates, for example 96.3% (6.0°C/min) vs 76.7% (5.5°C/min), respectively. Hence, nickel in the alloy accelerates reduction of the iron, presumably by more facile hydrogen activation.

Activation energies. Activation energies for the reduction reactions were determined using the standard temperature-programmed analysis (28) and by an Arrhenius analysis of peak parameters (5). The TPR results were more internally consistent and are reported in Table 10.

For Fe/SiO₂ the activation energy from the α peak is intermediate between the value of 26 ± 1 kcal/mole reported by Colombo *et al.* (24) for the surface reaction (either adsorption or dissociation of H₂ or reaction with O²⁻) and 55 kcal/mole, reported for the diffusion of iron cations in Fe₃O₄ (29). Thus, there is no single rate determining process here for the first reduction step. By contrast, E for the Fe₃O₄ \rightarrow α -Fe step is found to be 18.5 ± 1 kcal/mole, in relatively good agreement with the value of 15 ± 1 kcal/mole reported by Colombo *et al.* (24). The mechanism proposed for this step is that of nucleation and growth of the metal phase on the surface of the oxide.

Szekely *et al.* (26) report an activation energy for NiO reduction of 10.6 kcal/mole above the crystallographic transition tem-

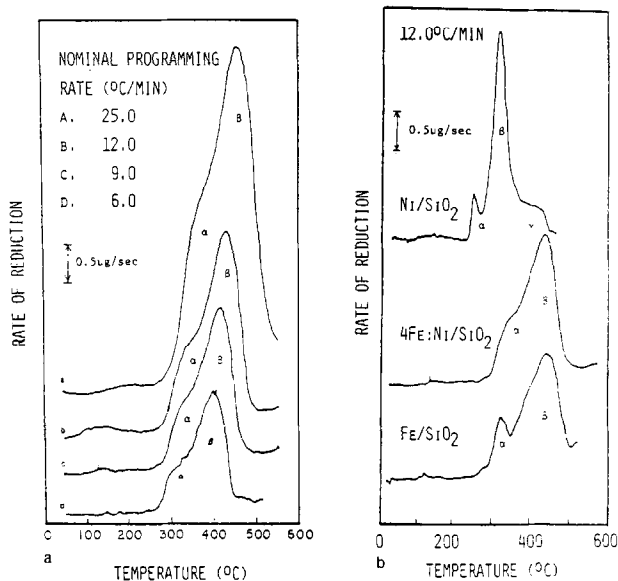


FIG. 12(a) Temperature programmed reduction of 4Fe : Ni/SiO₂. (b) Comparison of TPR profiles for the three catalysts.

perature of 259°C; above 310°C they report substantial bulk diffusional effects. The activation energy for diffusion of nickel cations in NiO is 49.5 kcal/mole, so, as in the case of the Fe/SiO₂ α peak, our value of 36.4 kcal/mole is bracketed by values pertaining to surface reaction and diffusionally limited processes.

For 4Fe : Ni/SiO₂ the activation energy could be determined reliably only for the β transition, 16.7 ± 3 kcal/mole. This compares with 18.5 ± 3 kcal/mole for Fe/SiO₂

TABLE 9

TPR Data for 4Fe : Ni/SiO₂

Profile	Peak	T (°C)	(-r) × 10 ² O ²⁻ /sec-nm ^{2a}	Percentage reduction at 485°C
A (25°C/min)	α	381 ± 20		76.4 ± 1
	β	462 ± 0.5	30.0 ± 1.5	
B (12°C/min)	α	350 ± 20		89.3 ± 1
	β	433 ± 0.5	18.4 ± 1.0	
C (9°C/min)	α	342 ± 20		93.9 ± 1
	β	421 ± 0.5	15.1 ± 1.0	
D (6°C/min)	α	320 ± 20		96.3 ± 1
	β	403 ± 0.5	11.0 ± 1.0	

^a Rates based on surface area of initial oxide catalyst.

TABLE 10

Activation Energies for the Reduction Reactions

Catalyst	Peak	Reaction	E (kcal/mole)	log ₁₀ μ (sec ⁻¹)
Fe/SiO ₂	α	Fe ₂ O ₃ → Fe ₃ O ₄	37.3 ± 4	11.06
Fe/SiO ₂	β	Fe ₃ O ₄ → α-Fe	18.5 ± 3	2.77
Ni/SiO ₂	β	NiO → Ni	36.4 ± 4	11.36
4 Fe : Ni/SiO ₂	β	Fe ₃₋₄ Ni ₆ O ₄ →	16.7 ± 3	2.63

β with similar frequency factors. Thus reduction of the iron appears to be the limiting factor for 4Fe : Ni/SiO₂, again leading to the conclusion of nickel acceleration of this step.

CONCLUSIONS

The Mössbauer effect, X-ray diffraction, and temperature-programmed reduction were used to study Fe/SiO₂, Ni/SiO₂, and 4Fe : Ni/SiO₂. Oxidation reduction sequences revealed that:

(1) The reduction of Fe₂O₃ in H₂ at 425°C to metallic iron proceeds through the intermediary Fe₃O₄ for small particles (≈ 15 nm) as for the bulk.

(2) Alloy formation in the 4Fe:Ni/SiO₂ occurs in the calcination stage and results in a mixed oxide.

(3) Reduction of the mixed 4Fe:Ni oxide in H₂ at 425°C yields a biphasic mixture of BCC and FCC alloys with the Ni-rich FCC phase containing approximately 37.5 atom%. Ni in agreement with the bulk equilibrium diagram.

(4) Reduction of NiO in H₂ at 425°C proceeds directly and completely to the metal.

(5) Activation energies for the reductions were measured using temperature-programmed gravimetry and found to be in agreement with bulk values for the Fe and Ni catalyts.

(6) The presence of Ni was found to accelerate the reduction in the 4Fe:Ni sample.

ACKNOWLEDGMENTS

The authors are indebted to Dow Chemical, USA, for support of this research through a Dow Central Research Fellowship in Catalysis, and to support via the Department of Energy, Office of Basic Energy Sciences, Division of Materials Sciences, Contract ER-78-S-02-4493. Mössbauer and X-ray studies were performed in the central facilities of the Northwestern Materials Research Center, supported by NSF-MRC, DMR 76-80847.

REFERENCES

- Amelse, J. A., Butt, J. B., and Schwartz, L. H., *J. Phys. Chem.* **82**, 558 (1978).
- Delgass, W. N., and Raupp, G. B., *J. Catal.*, **58**, 337 (1979).
- Unmuth, E. E., Ph.D. Dissertation, Northwestern University, Evanston, Illinois, June 1979.
- Cullity, B. D., "Elements of X-ray Diffraction." Addison-Wesley, New York, 1978.
- Falconer, J. C., and Madix, R. J., *Surf. Sci.* **48**, 393 (1975).
- Berry, L. G., ed., "Powdered Diffraction File, Inorganic," Sets 11-18, Joint Committee on Powder Diffraction Standards, Swarthmore, Pa., 1972.
- Muir, A. H., Ando, K. J., and Coogan, H. M., "Mössbauer Effect Data Index, 1958-1965." John Wiley, New York, 1966.
- Kündig, W., Ando, K. J., Lindquist, R. H., and Constabaris, G., *Czech. J. Phys.* **17**, 467 (1967).
- Kündig, W., Brommel, H., Constabaris, G., and Lindquist, R. H., *Phys. Rev.* **142**, 327 (1966).
- Meisel, W., Proc. 5th Int. Conf. Mössbauer Spectroscopy, Bratislava, Czech., p. 200, September 1973.
- Hobson, M. C., and Gager, H. M., *J. Catal.* **16**, 254 (1970).
- Hansen, M., "Constitution of Binary Alloys." 2nd ed. McGraw-Hill, New York, 1958.
- Vincze, I., Campbell, I. A., and Meyer, A. J., *Solid State Comm.* **15**, 14 (1974).
- Pearson, W. B., "Handbook of Lattice Spacings and Structure of Metals." Vol. 4. Pergamon Press, New York, 1958.
- Lebetter, H. M., and Reed, R. P., *J. Phys. Chem. Ref. Data* **2**, 531 (1974).
- Johnson, C. E., Ridout, M. S., and Cranshaw, T. E., *Proc. Phys. Soc.* **81**, 1079 (1963).
- We are indebted to Y-W. Chung for these measurements.
- Anderson, J. R., "Structure of Metallic Catalysts." Academic Press, New York, 1975.
- Sashital, S., Cohen, J. B., Burwell, R. L., Jr., and Butt, J. B., *J. Catal.* **50**, 479 (1977).
- Kofstad, P., "High Temperature Oxidation of Metals." John Wiley, New York, 1966.
- Levin, E. M., Robbins, C. R., and McMurdle, H. F., "Phase Diagrams for Ceramists." Am. Ceramic Soc., Columbus, OH, 1964.
- Arcuri, K., unpublished research.
- Gazzarini, F., and Lanzavecchia, G., Proc. 6th Int. Symp. on Reactivity of Solids, Schenectady, N.Y., August 1968.
- Colombo, Y., Gazzarini, F., and Lanzavecchia, G., *Mater. Sci. Eng.* **2**, 125 (1967).
- Keely, W. M., and Maynor, H. W., *J. Chem. Eng. Data* **8**, 297 (1968).
- Szekely, J., Lin, C. I., and Sohn, H. Y., *Chem. Eng. Sci.* **28**, 1975 (1973).
- Linnett, J. W., and Rahman, M. M., *J. Phys. Chem. Solids* **33**, 1465 (1972).
- Amenomiya, Y., and Cvetanovic, R. J., *J. Phys. Chem.* **67**, 144, 2046, 2705 (1963).
- Askill, J., "Tracer Diffusion Data for Metals, Alloys and Simple Oxides." Plenum, New York, 1970.